

# Spin Polarizabilities of the Nucleon from Polarized Low Energy Compton Scattering

Robert P. Hildebrandt<sup>a,1</sup>, Harald W. Grießhammer<sup>a,b,2</sup>  
and Thomas R. Hemmert<sup>a,b,3</sup>

<sup>a</sup> *Institut für Theoretische Physik (T39), Physik-Department,  
Technische Universität München, D-85747 Garching, Germany*

<sup>b</sup> *ECT\*, Villa Tambosi, I-38050 Villazzano (Trento), Italy*

## Abstract

As guideline for forthcoming experiments, we present predictions from Chiral Effective Field Theory for polarized cross sections in low energy Compton scattering for photon energies below 170 MeV, both on the proton and on the neutron. Special interest is put on the role of the nucleon spin polarizabilities which can be examined especially well in polarized Compton scattering. We present a model-independent way to extract their energy dependence and static values from experiment, interpreting our findings also in terms of the low energy effective degrees of freedom inside the nucleon: The polarizabilities are dominated by chiral dynamics from the pion cloud, except for resonant multipoles, where contributions of the  $\Delta(1232)$  resonance turn out to be crucial. We therefore include it as an explicit degree of freedom. We also identify some experimental settings which are particularly sensitive to the spin polarizabilities.

Suggested PACS numbers: 13.40.-f, 13.60.Fz, 14.20.Dh

Suggested Keywords: Effective Field Theory, Polarized Compton Scattering,  
Nucleon Spin Structure, Nucleon Polarizabilities.

---

<sup>1</sup>Email: rhildebr@ph.tum.de

<sup>2</sup>Email: hgrie@ph.tum.de; permanent address: a

<sup>3</sup>Email: themmert@ph.tum.de; permanent address: a

# 1 Introduction

Over the past few decades, real Compton scattering off the proton was established as an excellent tool to study the polarizabilities of the nucleon – theoretically as well as experimentally. A good overview over the various experiments is given in [1]; for an overlook of the theoretical studies cf. [2, 3] and references therein. As is well-known, polarizabilities are a measure for the stiffness of the nucleon in an external electric or magnetic field, caused by the displacement of the charged constituents of the nucleon, induced by the photon field. While the static values  $\bar{\alpha}_E$ ,  $\bar{\beta}_M$  of the two lowest (dipole) spin-independent polarizabilities are well understood, there are only few experiments which are able to extract the *spin polarizabilities* of the nucleon. These quantities have no simple classical analogon, as they parameterize the stiffness of the nucleon spin against electro-magnetically induced deformations relative to the axis defined by the nucleon spin. While there are four dipole spin polarizabilities for each nucleon [4], the only two quantities measured so far are the static forward and backward spin polarizabilities  $\gamma_0$  and  $\gamma_\pi$  of the proton.  $\gamma_0$  was extracted from the GDH experiment at MAMI, using a Dispersion Relation (DR) analysis [1, 5]:

$$\gamma_0 = (-1.01 \pm 0.13) \cdot 10^{-4} \text{ fm}^4 \quad (1.1)$$

A first attempt to determine  $\gamma_\pi$  from experiment by the LEGS group [6] quotes

$$\gamma_\pi = (-27.1 \pm 3.6) \cdot 10^{-4} \text{ fm}^4, \quad (1.2)$$

which is considerably lower than what one expected from DR analysis and Chiral Effective Field Theory ( $\chi$ EFT). An extraction from recent MAMI data, obtained at low energies [7] and in the region of the  $\Delta$  resonance [8, 9, 10], yields values which differ strongly (on a level of about 30%) from the LEGS value:

$$\begin{aligned} \gamma_\pi &= (-36.1 \pm 2.2) \cdot 10^{-4} \text{ fm}^4 & [7] \\ \gamma_\pi &= (-37.9 \pm 3.6) \cdot 10^{-4} \text{ fm}^4 & [8] \end{aligned} \quad (1.3)$$

These new results agree very well with the theoretical prediction from  $\chi$ EFT,

$$\gamma_\pi = -36.7 \cdot 10^{-4} \text{ fm}^4 \quad [11], \quad (1.4)$$

whereas calculations based on  $\chi$ EFT are at present not able to reproduce the MAMI value for  $\gamma_0$ , Eq. (1.1)<sup>1</sup>. For further details concerning experiments and their results see e.g. [1].

The goal of this work is to motivate further investigations of the spin polarizabilities, where there are still so many question marks left. Especially, we advocate double polarized experiments as a tool to dis-entangle the four leading spin polarizabilities, and not only the two static linear combinations given above.

Recently, it was demonstrated in [12] that nucleon polarizabilities can be connected to Compton multipoles and therefore also acquire a dependence on the energy  $\omega$  of the real,

---

<sup>1</sup>In the forward direction, a strong cancellation between two large spin polarizabilities makes accurate predictions for  $\gamma_0$  rather difficult [3].

incoming photon. These dispersion effects are well-known in solid state physics. In hadron structure physics different internal nucleonic degrees of freedom, low-lying nuclear resonances like the  $\Delta(1232)$ , the charged meson cloud around the nucleon etc., will react quite differently to real photon fields of non-zero frequency. Therefore, these *dynamical polarizabilities* contain detailed information about dispersive effects, caused by internal relaxation effects, baryonic resonances and mesonic production thresholds, see [12, 13] for details. As they stem from a multipole analysis of the scattering amplitude, dynamical polarizabilities contain all hadron structure information, but in a more readily accessible form. In the limit of zero photon energy, they reduce to the static polarizabilities mentioned above.

In principle, the dynamical polarizabilities are experimentally accessible by fits to Compton scattering cross sections. The main problem seems to be that the multipole expansion allows for an a priori infinite number of fit functions: The real photons can undergo transitions  $Tl \rightarrow T'l'$ , where  $T/T' = E$  or  $M$  labels the coupling of the incoming/outgoing photon as electric or magnetic, and  $l$ , ( $l' = l \pm \{0; 1\}$ ) is the angular momentum of the incident (outgoing) photon. Thus, there are six,  $\omega$ -dependent dipole polarizabilities, namely the two spin-independent ones  $\alpha_{E1}(\omega)$  and  $\beta_{M1}(\omega)$  for electric and magnetic dipole transitions which do not couple to the nucleon spin. In the spin sector there are the two diagonal polarizabilities  $\gamma_{E1E1}(\omega)$  and  $\gamma_{M1M1}(\omega)$  and the two off-diagonal spin polarizabilities  $\gamma_{E1M2}(\omega)$  and  $\gamma_{M1E2}(\omega)$ . In addition, there are higher ones like quadrupole and octupole polarizabilities. In [13], however, it was shown that one can describe unpolarized low energy Compton scattering off the proton very well by keeping only the  $l = 1$  (dipole) contributions of the Compton multipoles. This leaves us with six unknown functions of the photon energy that can be expressed as the six dynamical dipole polarizabilities.

Obviously, further experiments are needed to determine these six functions, as there is e.g. only a minor dependence on the spin polarizabilities visible in spin-averaged cross sections below the pion production threshold (see Sect. 5). Polarized Compton scattering experiments provide a new avenue for the determination of the six dipole polarizabilities. In the seminal paper [14] on polarized Compton scattering off a nucleon, an exhaustive list of interesting observables and asymmetries was defined which only now start to become accessible in this new frontier of low energy electromagnetic scattering experiments.

Guided by ongoing experimental feasibility studies at the HI $\gamma$ S lab of TUNL [15], we chose a subset of four asymmetries describing the interaction of circularly polarized photons with polarized protons and neutrons, where the polarization in the final states is not detected. We cover the low energy range, up to photon energies of  $\sim 170$  MeV, just above the one pion production threshold. Like in [14], we focus on asymmetries, dividing the difference of two polarized cross sections by their sum, as they are less sensitive to experimental errors than differences. Further investigations involving linearly polarized photon beams are under study [16]. We present predictions in the framework of Chiral Effective Field Theory with explicit  $\Delta$  degrees of freedom. Previously, a calculation of two of the asymmetries for polarized Compton scattering of the proton was presented to leading-one-loop order in a  $\chi$ EFT with only nucleon and pion degrees of freedom in [17]. In our analysis, (Sects. 6 and 7) we show a comparison between the two chiral frameworks for all asymmetries we consider, so that  $\Delta$  physics is easily identifiable. Since we investigate the possibility of

determining spin polarizabilities from experiment, we put special emphasis on the role of the spin and quadrupole ( $l = 2$ ) polarizabilities of the nucleon. The latter ones will – as in [13] for the spin-averaged case – turn out to be negligibly small, leaving only the six dynamical dipole polarizabilities as unknown structure parameters to be determined from data. As a starting point, one might consequently accept the theoretical findings for the spin-independent dipole polarizabilities  $\alpha_{E1}(\omega)$ ,  $\beta_{M1}(\omega)$ , for which  $\chi$ EFT and Dispersion analysis are in good agreement [13]. One would then attempt to extract the four dynamical  $l = 1$  spin polarizabilities directly from experiment, as will be described in Sect. 4.

In [14], the authors also investigated the energy dependence of various asymmetries both in a low energy expansion in terms of nucleon polarizabilities as well as in a full calculation in Dispersion Theory. The low energy expansion included the static values of the six dipole polarizabilities, the two static spin-independent quadrupole polarizabilities  $\bar{\alpha}_{E2}$ ,  $\bar{\beta}_{M2}$ , and the leading dispersion corrections to  $\bar{\alpha}_{E1}$  and  $\bar{\beta}_{M1}$ . Such a Taylor expansion of the polarizabilities is bound to break down as cusps or resonances are approached, the lowest of which being the one pion production threshold and the  $\Delta$  resonance. We will indeed find strong signals from the spin polarizabilities as the energy is increased. In contradistinction to [14], our calculation is based on *dynamical*, i.e. energy-dependent polarizabilities [12]. For photon energies above the pion production threshold, we expect our predictions only qualitatively to be correct, since the imaginary parts of our dynamical polarizabilities only correspond to tree-level accuracy and the width of the  $\Delta(1232)$  resonance is treated as a small perturbation; for details see [13]. Whereas the unpolarized cross sections were found to be well described up to 170 MeV within our theoretical framework [13], we have to caution the reader that this does not have to be the case for the asymmetries presented here, as these are much more sensitive on fine details.

The two spin configurations we investigate are described in Sect. 3, after a short repetition of the theoretical framework (Sect. 2). In Sect. 4, we propose a procedure to determine spin polarizabilities from experiment, before we have another look at spin-averaged cross sections in Sect. 5. The results for the proton asymmetries are presented and interpreted in Sect. 6, the ones for the neutron in Sect. 7. Conclusions and an Appendix on the two dominating Compton amplitudes complete the presentation.

## 2 Theoretical Framework

We calculate in the framework of Chiral Effective Field Theory with and without explicit  $\Delta(1232)$  degrees of freedom. Details concerning the former, Heavy Baryon Chiral Perturbation Theory (HB $\chi$ PT), which contains only pions and nucleons as explicit degrees of freedom, can be found e.g. in [17]. The formalism of the latter, called “Small Scale Expansion” (SSE) – an effective chiral field theory describing explicit pion, nucleon and  $\Delta(1232)$  degrees of freedom – is discussed in [18]. This work is based on the calculation of dynamical nucleon polarizabilities and spin-averaged Compton cross sections of the proton in [13] to which we refer the interested reader for details of our notation.

Real Compton scattering can be formulated in terms of six amplitudes<sup>2</sup>  $A_1 - A_6$ . The  $T$ -matrix reads

$$\begin{aligned}
T(\omega, z) = & A_1(\omega, z) \vec{\epsilon}'^* \cdot \vec{\epsilon} + A_2(\omega, z) \vec{\epsilon}'^* \cdot \hat{\vec{k}} \vec{\epsilon} \cdot \hat{\vec{k}}' \\
& + i A_3(\omega, z) \vec{\sigma} \cdot (\vec{\epsilon}'^* \times \vec{\epsilon}) + i A_4(\omega, z) \vec{\sigma} \cdot \left( \hat{\vec{k}}' \times \hat{\vec{k}} \right) \vec{\epsilon}'^* \cdot \vec{\epsilon} \\
& + i A_5(\omega, z) \vec{\sigma} \cdot \left[ \left( \vec{\epsilon}'^* \times \hat{\vec{k}} \right) \vec{\epsilon} \cdot \hat{\vec{k}}' - \left( \vec{\epsilon} \times \hat{\vec{k}}' \right) \vec{\epsilon}'^* \cdot \hat{\vec{k}} \right] \\
& + i A_6(\omega, z) \vec{\sigma} \cdot \left[ \left( \vec{\epsilon}'^* \times \hat{\vec{k}}' \right) \vec{\epsilon} \cdot \hat{\vec{k}}' - \left( \vec{\epsilon} \times \hat{\vec{k}} \right) \vec{\epsilon}'^* \cdot \hat{\vec{k}} \right]
\end{aligned} \tag{2.1}$$

with  $\hat{\vec{k}}$  ( $\hat{\vec{k}}'$ ) the unit vector in the momentum direction of the incoming (outgoing) photon with polarization  $\vec{\epsilon}$  ( $\vec{\epsilon}'^*$ ). We separate these amplitudes into pole ( $A_i^{\text{pole}}$ ) and non-pole ( $\bar{A}_i$ ) parts.

The non-pole amplitudes are also referred to as the structure part of the amplitudes. The question whether a contribution belongs to the structure part cannot be answered uniquely. In our definition, only those terms which have a pole either in the  $s$ -,  $u$ - or  $t$ -channel are treated as non-structure. If we were only concerned with the full calculation of Compton scattering cross sections, this separation clearly would be irrelevant because both, the structure dependent as well as the structure independent part, contribute. Here, however, we investigate the role of the internal nucleonic degrees of freedom on the spin and quadrupole polarizabilities in Compton scattering. Therefore, we need to be able to turn off and on the different nucleon polarizabilities, which are contained only in the structure part of the amplitudes.

Expressing the  $l = 1$  multipole expansion for nucleon Compton scattering in terms of dynamical dipole polarizabilities, one obtains

$$\begin{aligned}
\bar{A}_1(\omega, z) &= \frac{4\pi W}{M} [\alpha_{E1}(\omega) + z \beta_{M1}(\omega)] \omega^2 + \mathcal{O}(l = 2), \\
\bar{A}_2(\omega, z) &= -\frac{4\pi W}{M} \beta_{M1}(\omega) \omega^2 + \mathcal{O}(l = 2), \\
\bar{A}_3(\omega, z) &= -\frac{4\pi W}{M} [\gamma_{E1E1}(\omega) + z \gamma_{M1M1}(\omega) + \gamma_{E1M2}(\omega) + z \gamma_{M1E2}(\omega)] \omega^3 + \mathcal{O}(l = 2), \\
\bar{A}_4(\omega, z) &= \frac{4\pi W}{M} [-\gamma_{M1M1}(\omega) + \gamma_{M1E2}(\omega)] \omega^3 + \mathcal{O}(l = 2), \\
\bar{A}_5(\omega, z) &= \frac{4\pi W}{M} \gamma_{M1M1}(\omega) \omega^3 + \mathcal{O}(l = 2), \\
\bar{A}_6(\omega, z) &= \frac{4\pi W}{M} \gamma_{E1M2}(\omega) \omega^3 + \mathcal{O}(l = 2).
\end{aligned} \tag{2.2}$$

We choose to work in the centre-of-mass frame. Thus,  $\omega$  denotes the cm energy of the photon,  $M$  the isoscalar nucleon mass,  $W = \sqrt{s}$  the total cm-energy, and  $\theta$  the cm-scattering angle with  $z = \cos \theta$ .

---

<sup>2</sup>These amplitudes are different from the amplitudes  $A_i$  in [14], as we use a different basis.

The structure amplitudes  $\bar{A}_3 - \bar{A}_6$  contain only spin polarizabilities,  $\bar{A}_1 - \bar{A}_2$  only spin-independent ones. The spin polarizabilities  $\gamma_0$  ( $\gamma_\pi$ ) mentioned in the introduction are the leading coefficients of  $\bar{A}_3$  for  $\theta = 0^\circ$  ( $\theta = 180^\circ$ ) at zero energy:

$$\gamma_0 = -(\bar{\gamma}_{E1E1} + \bar{\gamma}_{M1M1} + \bar{\gamma}_{E1M2} + \bar{\gamma}_{M1E2}), \quad \gamma_\pi = -\bar{\gamma}_{E1E1} + \bar{\gamma}_{M1M1} - \bar{\gamma}_{E1M2} + \bar{\gamma}_{M1E2}$$

and do thus not suffice to determine the four leading spin polarizabilities completely. Here,  $\bar{\gamma}_i$  denotes the static limit  $\bar{\gamma}_i = \gamma_i(\omega = 0)$ . A precise definition of polarizabilities via the multipole expansion of the amplitudes is given in [13].

In the following, we list all the diagrams contributing in our leading-one-loop order ( $\mathcal{O}(\epsilon^3)$ ) calculation in the Small Scale Expansion, which contains the leading chiral dynamics of the pion cloud and the dominant  $\Delta$  physics with its pionic cloud.  $\epsilon$  is the expansion parameter of SSE and denotes either a small momentum, the pion mass or the mass difference between nucleon and  $\Delta(1232)$ . A diagram at a certain order in  $p$  containing pions in the theory without explicit  $\Delta$  degrees of freedom,  $\text{HB}\chi\text{PT}$ , contributes at the same order  $\epsilon$  in SSE.

In Fig. 1, we show the four  $\text{HB}\chi\text{PT}$  non-structure (pole) diagrams which contribute to an  $\mathcal{O}(p^3)$ - (and therefore also to an  $\mathcal{O}(\epsilon^3)$ -) calculation: the pole diagrams (a,b), the Thomson term (c) and the “pion pole” (d). The pole parts are thus given by the amplitudes of Compton scattering off a point-like nucleon with an anomalous magnetic moment, in addition to the  $\pi^0$ -pole contribution in the  $t$ -channel. In the literature, the latter contribution is sometimes classified as a structure part.

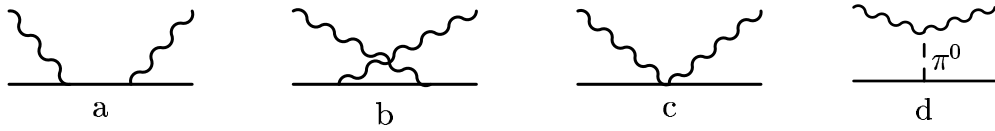


Figure 1: The diagrams identified as pole contributions at leading-one-loop order in  $\text{HB}\chi\text{PT}$ .

To  $\mathcal{O}(\epsilon^3)$ , one obtains now for the proton non-structure amplitudes

$$\begin{aligned} A_1^{\text{pole, p}}(\omega, \theta) &= -\frac{e^2}{M} + \mathcal{O}(\epsilon^4), \\ A_2^{\text{pole, p}}(\omega, \theta) &= \frac{e^2 \omega}{M^2} + \mathcal{O}(\epsilon^4), \\ A_3^{\text{pole, p}}(\omega, \theta) &= \frac{e^2 \omega (1 + 2 \kappa_p - (1 + \kappa_p)^2 \cos \theta)}{2 M^2} - \frac{e^2 g_A}{4 \pi^2 f_\pi^2} \frac{\omega^3 (1 - \cos \theta)}{m_{\pi^0}^2 + 2 \omega^2 (1 - \cos \theta)} + \mathcal{O}(\epsilon^4), \\ A_4^{\text{pole, p}}(\omega, \theta) &= -\frac{e^2 \omega (1 + \kappa_p)^2}{2 M^2} + \mathcal{O}(\epsilon^4), \\ A_5^{\text{pole, p}}(\omega, \theta) &= \frac{e^2 \omega (1 + \kappa_p)^2}{2 M^2} - \frac{e^2 g_A}{8 \pi^2 f_\pi^2} \frac{\omega^3}{m_{\pi^0}^2 + 2 \omega^2 (1 - \cos \theta)} + \mathcal{O}(\epsilon^4), \\ A_6^{\text{pole, p}}(\omega, \theta) &= -\frac{e^2 \omega (1 + \kappa_p)}{2 M^2} + \frac{e^2 g_A}{8 \pi^2 f_\pi^2} \frac{\omega^3}{m_{\pi^0}^2 + 2 \omega^2 (1 - \cos \theta)} + \mathcal{O}(\epsilon^4). \end{aligned} \quad (2.3)$$

The neutron pole amplitudes are

$$\begin{aligned}
A_1^{\text{pole, n}}(\omega, \theta) &= 0 + \mathcal{O}(\epsilon^4), \\
A_2^{\text{pole, n}}(\omega, \theta) &= 0 + \mathcal{O}(\epsilon^4), \\
A_3^{\text{pole, n}}(\omega, \theta) &= -\frac{e^2 \omega \kappa_n^2 \cos \theta}{2 M^2} + \frac{e^2 g_A}{4 \pi^2 f_\pi^2} \frac{\omega^3 (1 - \cos \theta)}{m_{\pi^0}^2 + 2 \omega^2 (1 - \cos \theta)} + \mathcal{O}(\epsilon^4), \\
A_4^{\text{pole, n}}(\omega, \theta) &= -\frac{e^2 \omega \kappa_n^2}{2 M^2} + \mathcal{O}(\epsilon^4), \\
A_5^{\text{pole, n}}(\omega, \theta) &= \frac{e^2 \omega \kappa_n^2}{2 M^2} + \frac{e^2 g_A}{8 \pi^2 f_\pi^2} \frac{\omega^3}{m_{\pi^0}^2 + 2 \omega^2 (1 - \cos \theta)} + \mathcal{O}(\epsilon^4), \\
A_6^{\text{pole, n}}(\omega, \theta) &= -\frac{e^2 g_A}{8 \pi^2 f_\pi^2} \frac{\omega^3}{m_{\pi^0}^2 + 2 \omega^2 (1 - \cos \theta)} + \mathcal{O}(\epsilon^4).
\end{aligned} \tag{2.4}$$

$\kappa_p$  ( $\kappa_n$ ) is the anomalous magnetic moment of the proton (neutron),  $e$  the proton's electric charge.  $m_{\pi^0}$  is the mass of the neutral pion,  $f_\pi$  the pion decay constant. The terms containing the axial coupling constant  $g_A$  are the contributions of the pion pole. The numerical values we use are listed in Table 1.

Parameter	Value	Comment	Source
$m_{\pi^0}$	135.0 MeV	neutral pion mass	[19]
$m_\pi$	139.6 MeV	charged pion mass	[19]
$M$	938.9 MeV	isoscalar nucleon mass	[19]
$f_\pi$	92.4 MeV	pion decay constant	[19]
$g_A$	1.267	axial coupling constant	[19]
$e$	$\sqrt{4 \pi / 137}$	electric charge of the proton	[19]
$\kappa_p$	1.793	anom. mag. moment proton	[19]
$\kappa_n$	-1.913	anom. mag. moment neutron	[19]

Table 1: Numerical values; magnetic moments are given in nuclear magnetons.

Fig. 2 shows the non-pole terms in leading-one-loop order  $\text{HB}\chi\text{PT}$  [20]. To this order, they contain only pion cloud effects around the nucleon. In SSE, the diagrams at order  $\epsilon^3$  in addition to the  $\text{HB}\chi\text{PT}$  ones of Figs. 1 and 2 are the  $\Delta$ - $\pi$ -continuum (Fig. 3), and  $\Delta$  pole diagrams (Figs. 4.1, 4.2) [11, 21]. We emphasize that there is no difference in the structure part of the amplitudes between proton and neutron up to  $\mathcal{O}(\epsilon^3)$ . Therefore, our non-pole amplitudes describe an isoscalar nucleon and the only difference between the two nucleons comes in via the pole amplitudes Eqs. (2.3, 2.4). As the analytic expressions for the structure amplitudes are rather lengthy, we refer the reader to [13] for a complete listing.

As discussed in [13] we require two additional operators – represented by the seagull graph in Fig. 4.3 – which are energy-independent and contribute only to the spin-independent dipole polarizabilities. These terms are formally  $\mathcal{O}(\epsilon^4)$ , but turn out to be

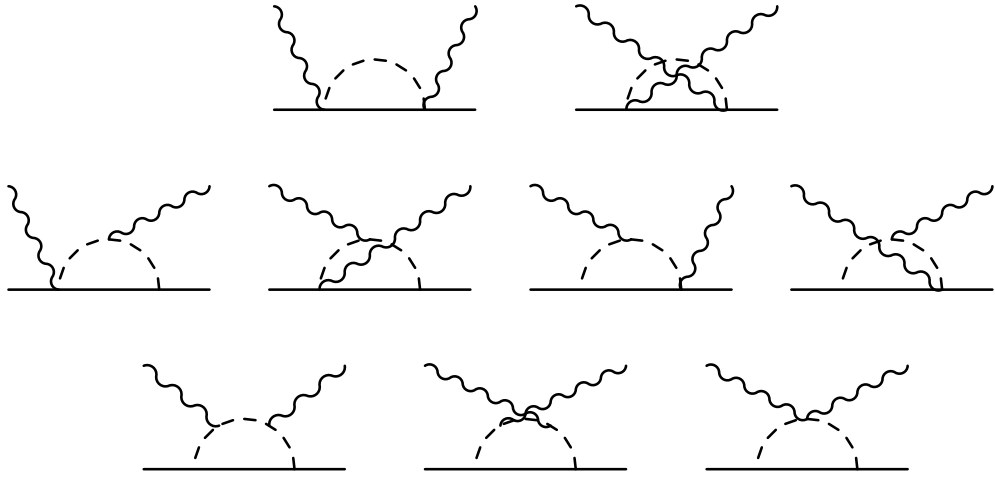


Figure 2: All diagrams contributing to the structure dependent amplitudes at leading-one-loop order in  $\text{HB}\chi\text{PT}$ .

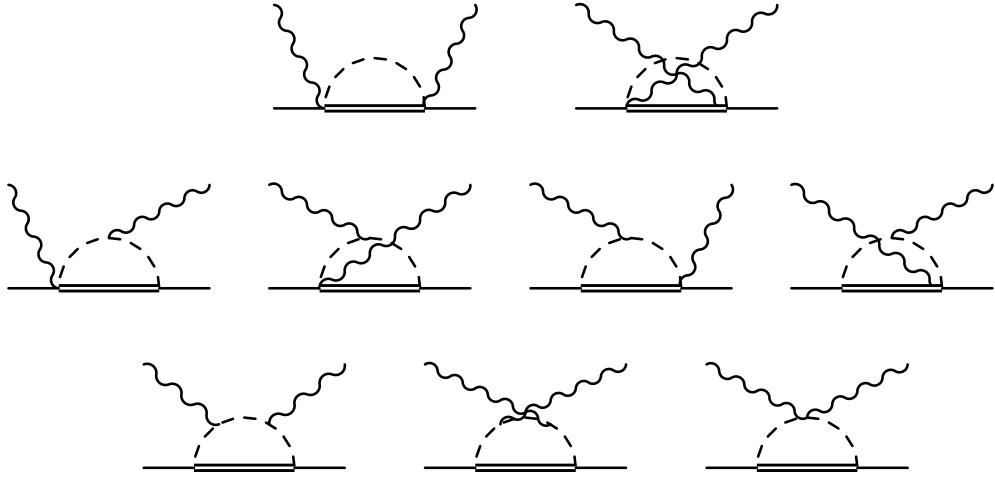


Figure 3: The  $\Delta$ - $\pi$ -continuum diagrams contributing at leading-one-loop order in SSE. The double line denotes the  $\Delta(1232)$ .

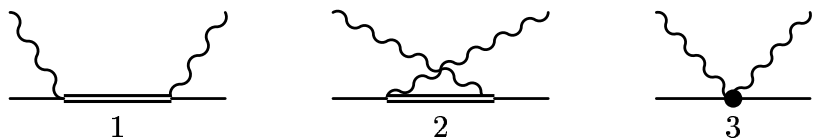


Figure 4:  $\Delta$  pole diagrams at leading-one-loop order and seagull graph.

anomalously large [13] and therefore have to be taken into account already at leading-one-loop order. Their numerical values are determined by a fit to unpolarized Compton scat-

tering data. The static, spin-independent dipole polarizabilities  $\bar{\alpha}_E$  and  $\bar{\beta}_M$  thus obtained are in excellent agreement to and of comparable uncertainty as the results from alternative extractions, see [13] for details.

We now turn to the formalism of Compton cross sections.

### 3 Cross Sections and Asymmetries – Formalism

The well-known formula for Compton cross sections in the cm frame is

$$\left. \frac{d\sigma}{d\Omega} \right|_{\text{cm}} = \left( \frac{M}{4\pi W} \right)^2 |T|^2. \quad (3.1)$$

In [13], we showed results for unpolarized proton cross sections, which are derived by averaging over the initial and summing over the final spin states. Now, we concentrate on spin-polarized cross sections for proton and neutron, albeit we will return briefly to spin-averaged ones in Sect. 5.

Triggered by a forthcoming proposal on polarized Compton scattering off  ${}^3\text{He}$  at the HI $\gamma$ S lab of TUNL [15], we choose the incoming photon to be right-circularly polarized,

$$\vec{\epsilon} = \frac{1}{\sqrt{2}} \begin{pmatrix} 1 \\ i \\ 0 \end{pmatrix}$$

and moving along the positive  $z$ -direction, while the final polarization and nucleon spin remain undetected. The two nucleon spin configurations we investigate are:

- 1) the difference between the target nucleon spin pointing parallel or antiparallel to the incident photon momentum

$$\frac{d\sigma_{\uparrow\uparrow}}{d\Omega_{\text{cm}}} - \frac{d\sigma_{\uparrow\downarrow}}{d\Omega_{\text{cm}}};$$

- 2) the difference between the target nucleon spin aligned in positive or negative  $x$ -direction:

$$\frac{d\sigma_{\uparrow\rightarrow}}{d\Omega_{\text{cm}}} - \frac{d\sigma_{\uparrow\leftarrow}}{d\Omega_{\text{cm}}}.$$

The corresponding formulae for  $|T|^2$  can already be found in [17], albeit there they are given only for real amplitudes  $A_1 - A_6$ . As is well-known, these amplitudes become complex for a photon energy above the pion production threshold  $\omega_\pi$ . Including the imaginary part of the amplitudes, the formulae read

$$\begin{aligned} \frac{1}{2} (|T|_{\uparrow\uparrow}^2 - |T|_{\uparrow\downarrow}^2) = & -\text{Re}[A_1 A_3^*] (1 + \cos^2 \theta) - \left[ |A_3|^2 + 2 |A_6|^2 + 2 |A_5|^2 \cos^2 \theta \right. \\ & + \text{Re}[A_6 (A_1^* + 3 A_3^*)] + \left( \text{Re}[A_3 (3 A_5^* + A_4^* - A_2^*)] + \text{Re}[A_5 (4 A_6^* - A_1^*)] \right) \cos \theta \\ & \left. + \text{Re}[A_5 (A_2^* - A_4^*)] \sin^2 \theta \right] \sin^2 \theta \end{aligned} \quad (3.2)$$

and

$$\begin{aligned}
\frac{1}{2} (|T|_{\uparrow\rightarrow}^2 - |T|_{\uparrow\leftarrow}^2) = & \left[ \text{Im}[A_1 (A_3^* + 2 A_6^* + 2 A_5^* \cos \theta)] \cos \theta + \text{Im}[A_1 A_4^*] (1 + \cos^2 \theta) \right. \\
& - \text{Im}[A_2 (A_3^* + 2 A_6^*)] \sin^2 \theta - \text{Im}[A_2 (A_4^* + 2 A_5^*)] \cos \theta \sin^2 \theta \Big] \sin \theta \sin \phi \\
& + \left[ \text{Re}[A_3 (A_3^* - A_1^* + 2 A_6^*)] \cos \theta + \text{Re}[A_3 A_5^*] (3 \cos^2 \theta - 1) \right. \\
& + \left( \text{Re}[A_1 A_5^*] + \text{Re}[A_2 A_3^*] + \text{Re}[A_6 (A_2^* + A_4^* - 2 A_5^*)] \right) \sin^2 \theta \\
& \left. + \text{Re}[A_3 A_4^*] (\cos^2 \theta + 1) + \text{Re}[A_5 (A_2^* - A_4^* - 2 A_5^*)] \cos \theta \sin^2 \theta \right] \sin \theta \cos \phi . \tag{3.3}
\end{aligned}$$

Here,  $\phi$  is the angle between the reaction plane and the plane spanned by the momentum of the incoming photon and the target nucleon spin. Obviously, the difference Eq. (3.3) takes on the largest values – at least below the pion production threshold – for  $\phi = 0$ . Therefore, we choose the nucleon spin in the reaction plane, which simplifies Eq. (3.3) considerably. Using left- instead of right-circularly polarized photons changes only the overall sign in Eq. (3.2) and Eq. (3.3).

For comparison, we show once again  $|T|^2$  for the spin-averaged cross section [17], which can be derived by taking the sum instead of the difference in Eq. (3.2) (or as well in Eq. (3.3)):

$$\begin{aligned}
\frac{1}{2} (|T|_{\uparrow\uparrow}^2 + |T|_{\uparrow\downarrow}^2) = & \frac{1}{2} |A_1|^2 (1 + \cos^2 \theta) + \frac{1}{2} |A_3|^2 (3 - \cos^2 \theta) + \left[ \frac{1}{2} |A_4|^2 (1 + \cos^2 \theta) \right. \\
& + \frac{1}{2} |A_2|^2 \sin^2 \theta + |A_5|^2 (1 + 2 \cos^2 \theta) + 3 |A_6|^2 + 4 \text{Re}[A_3 A_6^*] + 2 \text{Re}[A_4 A_5^*] \cos^2 \theta \\
& \left. + \left( -\text{Re}[A_1 A_2^*] + \text{Re}[A_3 (A_4^* + 2 A_5^*)] + 2 \text{Re}[A_6 (A_4^* + 3 A_5^*)] \right) \cos \theta \right] \sin^2 \theta \tag{3.4}
\end{aligned}$$

The asymmetries we consider<sup>3</sup> are

$$\Sigma_z = \frac{|T|_{\uparrow\uparrow}^2 - |T|_{\uparrow\downarrow}^2}{|T|_{\uparrow\uparrow}^2 + |T|_{\uparrow\downarrow}^2} , \tag{3.5}$$

$$\Sigma_x = \frac{|T|_{\uparrow\rightarrow}^2 - |T|_{\uparrow\leftarrow}^2}{|T|_{\uparrow\rightarrow}^2 + |T|_{\uparrow\leftarrow}^2} . \tag{3.6}$$

$\Sigma$  is a frame independent quantity, as the frame dependent flux factor cancels in the ratio between difference and sum of the cross section, while  $|T|^2$  can be written in terms of the frame independent Mandelstam variables.

---

<sup>3</sup> $\Sigma_z$  corresponds to  $\Sigma_{2z}$  in the notation of [14],  $\Sigma_x$  to  $\Sigma_{2x}$ .

From the experimentalist's point of view, it is more convenient to measure the *asymmetry* – i.e. the difference divided by the sum – instead of the differences Eq. (3.2) and Eq. (3.3), as the former is more tolerant to systematic errors in experiments. Nevertheless, division by a small quantity, say a small spin-averaged cross section, may enhance theoretical uncertainties. Sensitivity on the nucleon structure, e.g. the nucleon spin, may be lost by dividing the difference by the sum, as we will see a few times in Sects. 6 and 7. We therefore give also two more definitions which abbreviate the cm differences:

$$\mathcal{D}_z = \frac{1}{2} \left( \frac{d\sigma_{\uparrow\uparrow}}{d\Omega_{\text{cm}}} - \frac{d\sigma_{\uparrow\downarrow}}{d\Omega_{\text{cm}}} \right) \quad (3.7)$$

$$\mathcal{D}_x = \frac{1}{2} \left( \frac{d\sigma_{\uparrow\rightarrow}}{d\Omega_{\text{cm}}} - \frac{d\sigma_{\uparrow\leftarrow}}{d\Omega_{\text{cm}}} \right) \quad (3.8)$$

## 4 Extracting Spin Polarizabilities from Experiment

A first step in determining dynamical spin polarizabilities from experiment might be to accept our findings for the spin-independent dipole polarizabilities  $\alpha_{E1}(\omega)$  and  $\beta_{M1}(\omega)$ , which show very good agreement with Dispersion Relation analysis up to about 170 MeV [13]. Truncating at  $l = 1$ , this leaves no unknowns in  $A_1$  and  $A_2$ . As higher polarizabilities are negligible, the spin-dependent dipole polarizabilities could then be fitted to data sets which combine polarized and spin-averaged experimental results, taken at a fixed energy and varying the scattering angle. As starting values for the fit, one might use our  $\chi$ EFT-results [13], as indicated in Eq. (4.1), where we show the spin structure amplitudes up to  $l = 1$  with the polarizabilities  $\gamma_i(\omega)$  replaced by  $\gamma_i(\omega) + \delta_i$ , introducing the fit parameters  $\delta_i$ . Small fit parameters mean correct prediction of the dynamical spin dipole polarizabilities within the Small Scale Expansion.

$$\begin{aligned} \bar{A}_3^{\text{fit}}(\omega, z) &= -\frac{4\pi W}{M} [(\gamma_{E1E1}(\omega) + \delta_{E1E1}) + z(\gamma_{M1M1}(\omega) + \delta_{M1M1}) \\ &\quad + (\gamma_{E1M2}(\omega) + \delta_{E1M2}) + z(\gamma_{M1E2}(\omega) + \delta_{M1E2})] \omega^3 \\ \bar{A}_4^{\text{fit}}(\omega, z) &= \frac{4\pi W}{M} [-(\gamma_{M1M1}(\omega) + \delta_{M1M1}) + (\gamma_{M1E2}(\omega) + \delta_{M1E2})] \omega^3 \\ \bar{A}_5^{\text{fit}}(\omega, z) &= \frac{4\pi W}{M} (\gamma_{M1M1}(\omega) + \delta_{M1M1}) \omega^3 \\ \bar{A}_6^{\text{fit}}(\omega, z) &= \frac{4\pi W}{M} (\gamma_{E1M2}(\omega) + \delta_{E1M2}) \omega^3 \end{aligned} \quad (4.1)$$

Thus, one obtains the spin dipole polarizabilities at a definite energy. Repeating this procedure for various energies gives the energy dependence, i.e. the dynamics of the  $l = 1$  spin polarizabilities. Therefore, the amplitudes Eq. (4.1) provide one possible way to extract dynamical spin polarizabilities directly from the asymmetry observables of the previous section, using  $\chi$ EFT. Note that the  $\delta_i$  may show a weak energy dependence. At first trial, they can be taken as energy-independent quantities. This corresponds to a free normalization of

the spin dipole polarizabilities, assuming the energy dependence derived from  $\chi$ EFT to be correct. This assumption is well justified, as at low energies only  $\Delta(1232)$  and pion degrees of freedom are supposed to give dispersive contributions to the polarizabilities.

## 5 Spin Contributions to Spin-Averaged Cross Sections

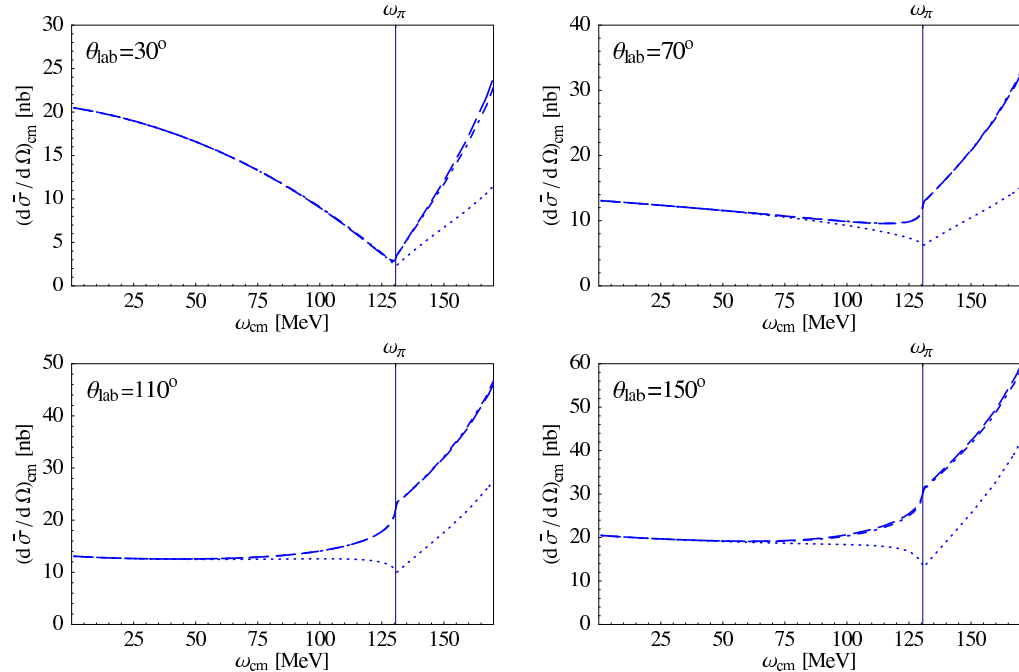


Figure 5: Complete  $\mathcal{O}(\epsilon^3)$ -SSE-predictions (dashed) for the spin-averaged proton cross section; dotted: spin polarizabilities not included, dotdashed: quadrupole polarizabilities not included.

Before discussing the asymmetries in detail, we briefly turn to the question which polarizabilities are seen in unpolarized Compton cross sections, discussing the  $\mathcal{O}(\epsilon^3)$  SSE-results partially given already in [13]. As shown in Fig. 5, we find a large contribution of the dynamical spin polarizabilities to spin-averaged Compton cross sections on the proton above  $\omega \sim 100$  MeV. We also show our so far unpublished results for the neutron (Fig. 6), exhibiting a huge sensitivity on the spin polarizabilities in the backward direction. This can be well understood, as the right hand side of Eq. (3.4) simplifies to  $|A_1|^2 + |A_3|^2$  for  $\theta = 0^\circ$  and  $\theta = 180^\circ$ . In the forward direction, the spin-independent amplitude  $|A_1|^2$  dominates, in backward direction the spin-dependent amplitude  $|A_3|^2$ , as can be seen in App. A.

We note also again that any effects of quadrupole polarizabilities are invisible at the level of the unpolarized cross sections, as has already been found in [13] for the proton. It suffices therefore to terminate the multipole expansion Eq. (2.2) at the dipole level, which leaves the six dipole polarizabilities as parameters.

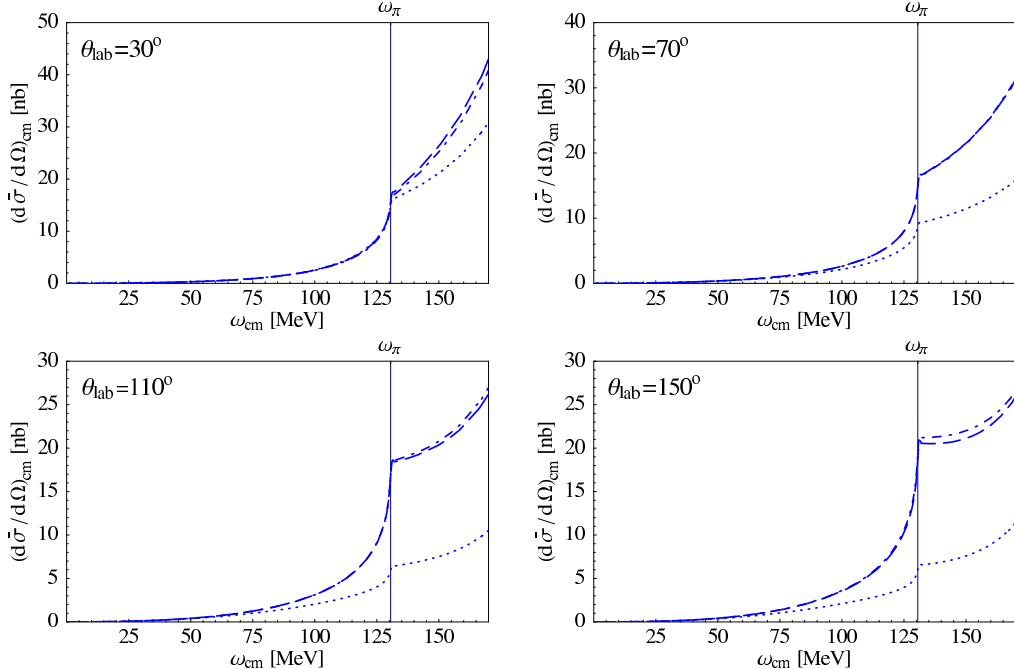


Figure 6: Complete  $\mathcal{O}(\epsilon^3)$ -SSE-predictions (dashed) for the spin-averaged neutron cross section; dotted: spin polarizabilities not included, dotdashed: quadrupole polarizabilities not included.

While effects from the spin polarizabilities are non-negligible in unpolarized experiments, to extract all four of them from such data is clearly illusory. Thus, double polarized experiments as discussed in the rest of this article are necessary additional ingredients in a combined multipole analysis.

## 6 Proton Asymmetries

We therefore turn now to the results for the asymmetries of the proton. Analogously to the previous section, we will confirm for each observable that the quadrupole polarizabilities are negligible. Thus, the multipole expansion of the amplitude can always be truncated at the dipole level, leaving at most six parameters. However, it will turn out that not all asymmetries are equally sensitive on the spin polarizabilities. As expected, most asymmetries are indeed governed by the pole part of the amplitudes.

In order to determine which asymmetries are most sensitive to the structure parts of the Compton amplitudes, and which of the internal low energy degrees of freedom in the nucleon dominate the structure dependent part of the cross section, we will first compare three scenarios for each asymmetry: (i) the result when only the pole terms of the amplitudes are kept; (ii) the same when the effects from the pion cloud around the nucleon are added, as described by the leading-one-loop order HB $\chi$ PT result; and finally (iii) a leading-one-loop

order calculation in SSE, including also the  $\Delta$  as dynamical degree of freedom.

An ideal asymmetry should thus fulfill three criteria: It should be large to give a good experimental signal, it should show sensitivity on the structure amplitudes, and it should allow a differentiation between the pion cloud and  $\Delta$  resonance contributions in resonant channels, revealing as much as possible about the role of at least these low energy degrees of freedom in the nucleon. In Sect. 7, we will repeat this presentation for the neutron asymmetries. To simplify connection to experiment, we give the scattering angle in the following plots in the lab-frame.

Similar plots for the nucleon asymmetries are already shown in [14], using Dispersion Theory techniques. Direct comparison to those plots is however not possible because of a different choice of angles – the authors of [14] concentrated on the extreme angles  $0^\circ$ ,  $90^\circ$ ,  $180^\circ$ , whereas we cover the whole experimentally accessible angular spectrum. Nevertheless, qualitative agreement between our  $\chi$ EFT results and [14] can be deduced.

We emphasize also that our predictions are parameter-free, as all constants are determined from unpolarized Compton scattering on the proton, [13]. In the following the fit parameters  $\delta_i$  introduced in Eq. (4.1) are all set to zero, as no measured asymmetries exist at this point.

## 6.1 Nucleon Spin Parallel Photon Momentum

### 6.1.1 Comparison: Pole-, HB $\chi$ PT- and SSE-calculation of $\Sigma_z^p$

As one can see in Fig. 7, the proton asymmetry  $\Sigma_z^p$  reaches values of  $\mathcal{O}(1)$  and is therefore quite large, although it vanishes for  $\omega = 0$ , due to the vanishing difference and the finite static spin-averaged cross section, given by the familiar Thomson-limit. This is valid independently of the scattering angle.

Comparing the three curves in Fig. 7 – third order pole,  $\mathcal{O}(p^3)$ -HB $\chi$ PT and  $\mathcal{O}(\epsilon^3)$ -SSE – one recognizes the strong influence of the pole amplitudes, given by Eq. (2.3). This is exactly what one expects for the charged proton, and can also be deduced from Eqs. (2.2, 2.3, 3.2): The asymmetry starts linearly in  $\omega$ , while the leading term of the structure part of  $\Sigma_z^p$  is proportional to  $\omega^3$ , as there is no term in Eq. (3.2) that contains only spin-independent amplitudes. As we are interested in information about the structure of the nucleon, i.e. in the deviation of the dashed lines from the solid (pole contributions only) line in Fig. 7, and as this deviation is not as strong as later in  $\Sigma_x^p$  and in the neutron asymmetries,  $\Sigma_z^p$  does not seem to be the ideal choice among the considered quantities to examine the nucleon structure.

Concerning the explicit  $\Delta$  degrees of freedom, we see sizeable contributions only above  $\omega_\pi$ . The only exception is noticed in extreme forward direction, but this is an artifact of the asymmetry, which is extremely sensitive at small angles due to the small spin-averaged cross section at  $\omega_\pi$  (Fig. 5), and neither visible in the difference  $\mathcal{D}_z$  nor in the spin-averaged cross section.

The structure of  $\Sigma_z^p$  varies a lot for the different angles. It is negative in forward and positive in backward direction. This can be explained – at least for low energies ( $\leq 120$

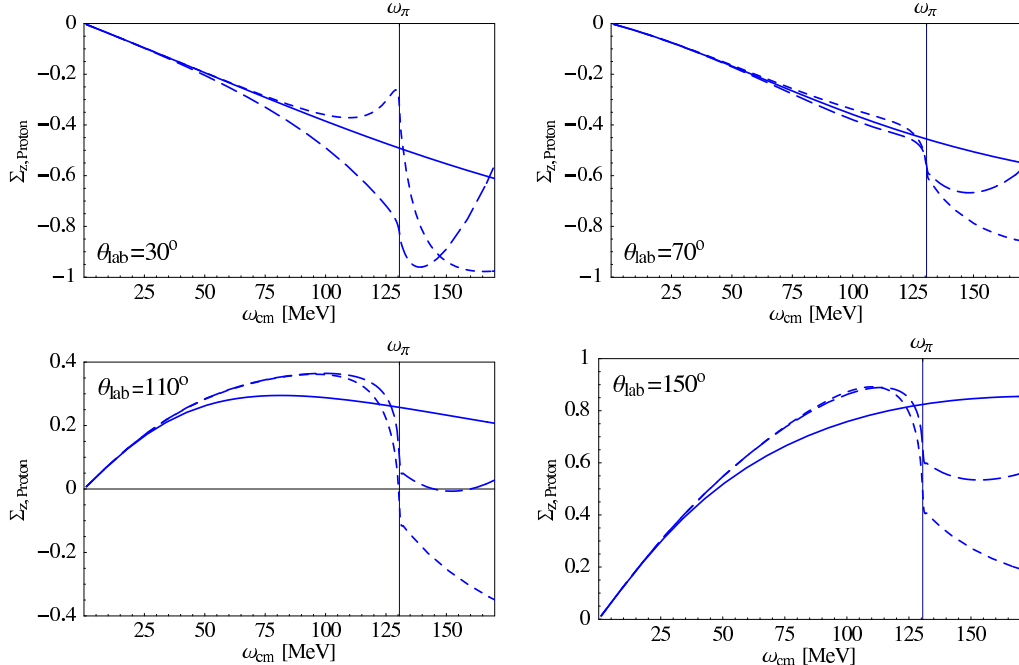


Figure 7:  $\mathcal{O}(p^3)$ -HB $\chi$ PT- (shortdashed) and  $\mathcal{O}(\epsilon^3)$ -SSE-predictions (longdashed) for the proton asymmetry  $\Sigma_z^p$ ; the solid line describes the third order pole contributions.

MeV) – looking at the amplitudes  $A_1$  and  $A_3$  in Fig. 19 because for  $\theta = 0^\circ$  and  $\theta = 180^\circ$  the right hand side of Eq. (3.2) reduces to  $-2 A_1 A_3$ . The proton amplitude  $A_3$  starts with a falling slope in forward and with a rising slope in backward direction, while  $A_1$  is negative below the pion production threshold for all angles under consideration. The spin-averaged cross section is positive for all angles and energies by definition.

At  $\omega_\pi \approx 131$  MeV in the cm system, the cusp at the pion production threshold is clearly visible for most of the angles. This cusp arises since the amplitudes become complex at the threshold. Polarized cross sections are much more sensitive on the fine structure of the nucleon than their unpolarized pendants. Therefore, our results might considerably deviate from experiment above threshold, due to sizeable uncertainties in our imaginary parts. Nevertheless, qualitative agreement should be fulfilled, so we use the same plot range as for the unpolarized results in [13], with a maximum photon energy of 170 MeV. In [14], the plots end below threshold since its low energy expansion of the polarizabilities cannot reproduce the non-analyticity of the pion production threshold.

### 6.1.2 Spin and Quadrupole Contributions to $\Sigma_z^p$

The asymmetry (Fig. 8), and especially the difference (Fig. 9), exhibit only a weak dependence on the spin polarizabilities in forward direction below  $\omega_\pi$ , which is no surprise, as in Fig. 19 there are nearly no structure contributions to  $A_3^p$  visible below 100 MeV. In the backward direction, the sensitivity on the  $\gamma_i$ 's is large, especially in the difference.

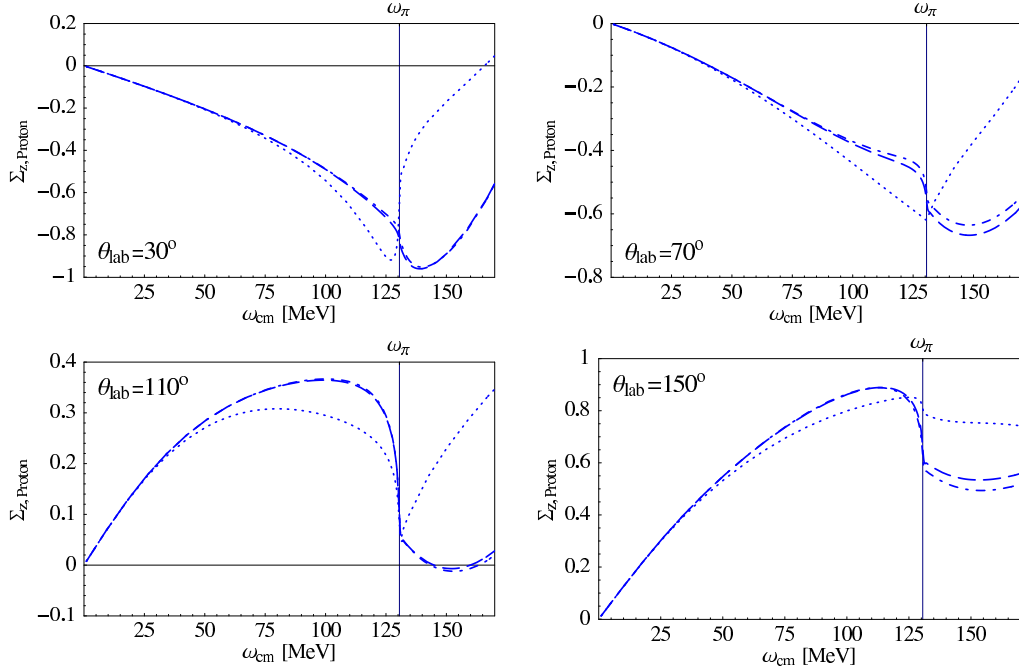


Figure 8: Complete  $\mathcal{O}(\epsilon^3)$ -SSE-predictions (dashed) for the proton asymmetry  $\Sigma_z^p$ ; dotted: spin polarizabilities not included, dotdashed: quadrupole polarizabilities not included.

The sharp rise of the result without spin polarizabilities in Fig. 8 above the pion production threshold in forward direction is due to the sharply rising difference and the small spin-averaged cross section which enters the denominator presented in Fig. 5.

In the literature, e.g. in [6], the pion pole (Fig 1.d) is often considered as one of the structure diagrams, giving a contribution to the static backward spin polarizability  $\gamma_\pi$ , which is much larger than all the other contributions. We treat the term as pole, as it contains a pion pole in the  $t$ -channel. So the question arises why we are sensitive to the spin polarizabilities, despite of having removed this supposedly dominant part from them. The reason is that the pion pole dominates over the structure part of  $\gamma_\pi$  only for low energies. The pion pole contribution to  $\gamma_\pi(\omega)$  describes a Lorentzian (Eq. (2.3)) and becomes smaller than the structure contribution above 100 MeV, as the latter one rises due to the increasing values of  $\gamma_{E1E1}(\omega)$  and  $\gamma_{M1M1}(\omega)$  [13].

It is crucial to notice that the quadrupole polarizabilities ( $l = 2$ ) play again a negligibly small role, see Figs. 8 and 9. The most important quadrupole contribution is observed at  $70^\circ$  and  $150^\circ$ , but the relative size is still  $< 0.1$  and therefore presumably within the experimental error bars. As repeatedly stated, that these contributions are small is mandatory if one wants to determine spin polarizabilities via polarized cross section data, because only then can the multipole expansion be truncated at  $l = 1$  as in Eqs. (2.2, 4.1).

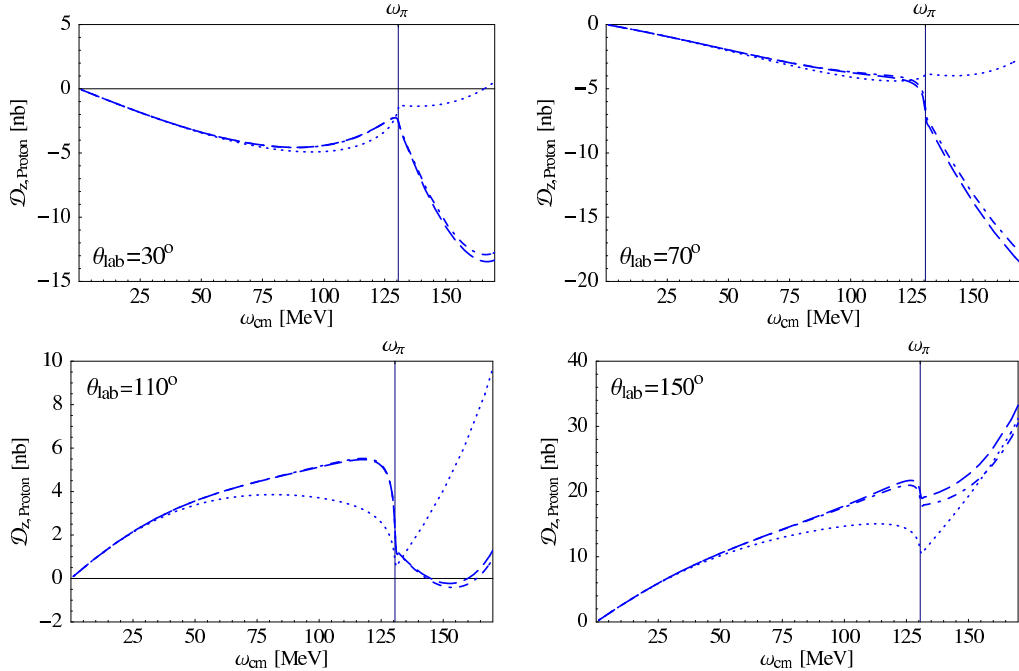


Figure 9: Complete  $\mathcal{O}(\epsilon^3)$ -SSE-predictions (dashed) for the proton difference  $\mathcal{D}_z^p$ ; dotted: spin polarizabilities not included, dotdashed: quadrupole polarizabilities not included.

## 6.2 Nucleon Spin Perpendicular to Photon Momentum

### 6.2.1 Comparison: Pole-, HB $\chi$ PT- and SSE-calculation of $\Sigma_x^p$

The asymmetry  $\Sigma_x^p$  in Fig. 10 looks quite similar for the different angles: It always starts with a falling slope and exhibits a sharp minimum at the pion cusp, therefore staying negative in a wide energy range. This behavior is no surprise, as the leading term in Eq. (3.3) for the proton for  $\theta \approx 0^\circ$ ,  $\theta \approx 180^\circ$ , i.e.  $\sin^2 \theta \approx 0$ , is  $A_3 (A_3 - A_1) \sin \theta \cos \theta$ , which is the only term including  $A_1$  and therefore dominating for low energies, as  $A_1^p$  contains the Thomson-limit. In both forward and backward direction  $A_3 - A_1 > 0$ , and  $A_3 < (>) 0$  for small (large) angles and low energies. The factor  $\cos \theta$  gives an additional minus sign in backward direction.

Even more striking than for  $\Sigma_z^p$  is the weak sensitivity of the asymmetry  $\Sigma_x^p$  on explicit  $\Delta$  degrees of freedom. Once again, the only exception to this rule is the extreme forward direction because of the small spin-averaged cross section which enhances the small deviations between the HB $\chi$ PT- and the SSE-calculation of the difference  $\mathcal{D}_x^p$  and makes  $\Sigma_x^p$  extremely sensitive on errors. Therefore, we consider the forward angle regime as inconvenient for measuring proton asymmetries. In the other panels of Fig. 10 the  $\Delta$ -dependence cancels in the asymmetry, whereas we found the  $\Delta(1232)$  resonance to give sizeable contributions to both the difference and the sum. This is one example that an asymmetry actually hides interesting physical information.

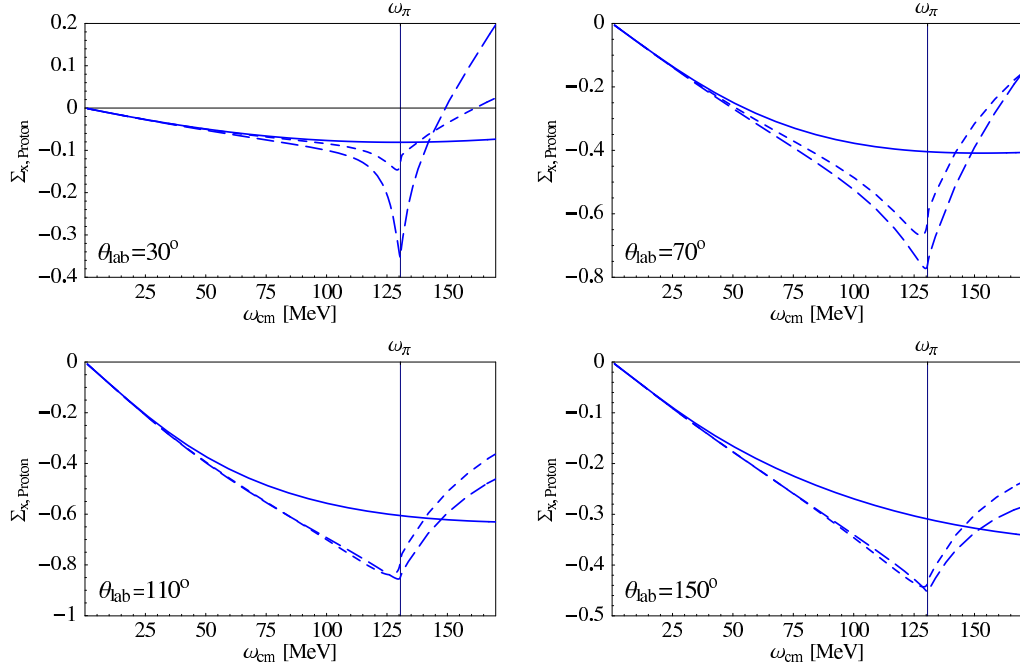


Figure 10:  $\mathcal{O}(p^3)$ -HB $\chi$ PT- (shortdashed) and  $\mathcal{O}(\epsilon^3)$ -SSE-predictions (longdashed) for the proton asymmetry  $\Sigma_x^p$ ; the solid line describes the third order pole contributions.

The dominance of the pole amplitudes is – as in  $\Sigma_z^p$  – clearly visible. The argument is the same as the one given in Sect. 6.1. Nonetheless, we find  $\Sigma_x^p$  more sensitive on the nucleon structure than  $\Sigma_z^p$ , especially around  $\omega_\pi$ .

### 6.2.2 Spin and Quadrupole Contributions to $\Sigma_x^p$

As one can see in Figs. 11 and 12,  $\Sigma_x^p$  and  $\mathcal{D}_x^p$  are very sensitive on the spin polarizabilities for all angles. Therefore – and because of our findings in the previous subsection – this configuration (nucleon spin perpendicular to the photon momentum) seems to be more convenient than spin parallel photon momentum, to examine the spin structure of the nucleon. In the backward direction, the spin dependence of the asymmetry is less pronounced than in forward direction.

The quadrupole contributions are extremely small.

## 7 Neutron Asymmetries

In the absence of stable single neutron targets, the following results for the neutron have to be corrected for binding and meson exchange effects inside light nuclei, a task which will be the scope of future work. Here, we present the neutron results to guide considerations on future experiments using polarized deuterium or  $^3\text{He}$ , e.g. [15].

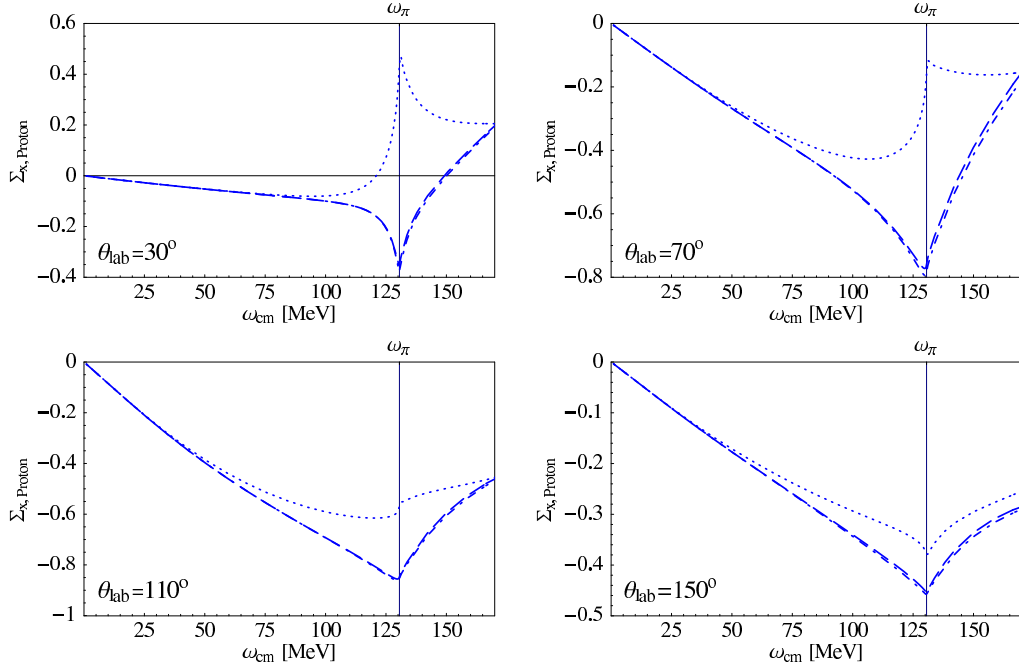


Figure 11: Complete  $\mathcal{O}(\epsilon^3)$ -SSE-predictions (dashed) for the proton asymmetry  $\Sigma_x^p$ ; dotted: spin polarizabilities not included, dotdashed: quadrupole polarizabilities not included.

As in the proton case, the neutron asymmetries reach quite large values of  $\mathcal{O}(1)$  as the photon energy increases. In the neutron, pole contributions might be expected to be small, because it is uncharged and thus only the pion pole and anomalous magnetic moment contribute. On the other hand, spin polarizabilities are then not enhanced by interference with large pole amplitudes. Therefore, whether and which neutron asymmetries are sensitive to the structure parts, and hence to the  $\gamma_i$ 's, must be investigated carefully.

We follow the same line of presentation as outlined at the beginning of Sect. 6 for the proton asymmetries: First, we investigate which internal degrees of freedom are seen in a specific asymmetry, and then show that quadrupole polarizabilities give negligible contributions. Thus, the asymmetries most sensitive to spin polarizabilities are identified.

## 7.1 Nucleon Spin Parallel Photon Momentum

### 7.1.1 Comparison: Pole-, HB $\chi$ PT- and SSE-calculation of $\Sigma_z^n$

Comparing Fig. 13 to the proton analogs, Figs. 7 and 10, we notice that the neutron is much more sensitive on the structure amplitudes. The pole curves show only a weak energy-dependence, so that nearly the whole dynamics is given by the neutron polarizabilities. This minor influence of the pole amplitudes is due to the vanishing third order pole contributions to  $A_1$  and  $A_2$ , which make the difference Eq. (3.2) start with a term proportional to  $\omega^2$ , whereas the leading structure part is  $\mathcal{O}(\omega^3)$ . The spin-averaged cross section starts with

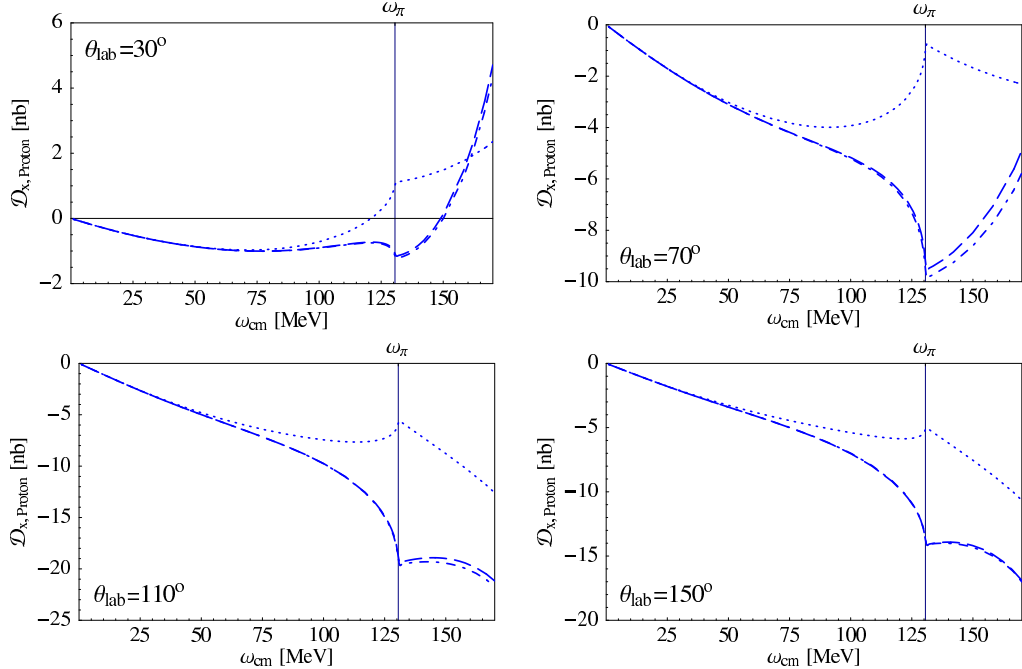


Figure 12: Complete  $\mathcal{O}(\epsilon^3)$ -SSE-predictions (dashed) for the proton difference  $\mathcal{D}_x^p$ ; dotted: spin polarizabilities not included, dotdashed: quadrupole polarizabilities not included.

$\omega^2$ , rendering finite static values of  $\Sigma_z^n$ . The angular dependence of this static value can be derived from Eqs. (2.4, 3.2, 3.4) as

$$\Sigma_z^n(\omega = 0, \theta) = \frac{4 \sin^2 \theta}{-5 + \cos(2\theta)} . \quad (7.1)$$

The structure sensitivity of the neutron is also visible in the huge sensitivity of  $\Sigma_z^n$  to the  $\Delta$  resonance which influences the polarized cross sections considerably even for very low energies. As is well-known, the influence of the  $\Delta(1232)$  increases with increasing angle.

Concerning the shape of the asymmetry, one recognizes a similar behaviour for the whole angular spectrum. It always reaches a local minimum at the pion cusp. A precise interpretation of the shape of  $\Sigma_z^n$  is hard to give, as the denominator has the leading power  $\omega^2$ , while it was  $\omega^0$  in the proton case. Therefore, it is more instructive to look at the difference (Fig. 15). For small angles this quantity first rises, while in backward direction it becomes negative from the very beginning. The reason is perfectly clear from the amplitudes  $A_1$  and  $A_3$  in App. A, as the product  $A_1 \cdot A_3$  is negative for low energies in forward direction, positive in backward direction. Recall that for the neutron,  $A_1 = \bar{A}_1$  contains only structure contributions, Eq. 2.3.

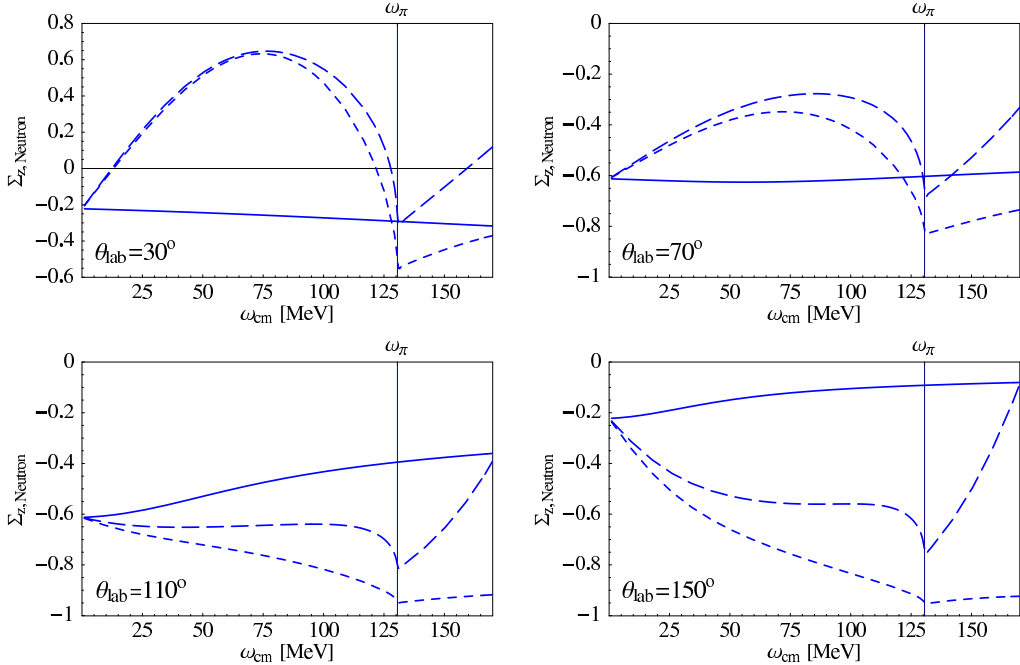


Figure 13:  $\mathcal{O}(p^3)$ -HB $\chi$ PT- (shortdashed) and  $\mathcal{O}(\epsilon^3)$ -SSE-predictions (longdashed) for the neutron asymmetry  $\Sigma_z^n$ ; the solid line describes the third order pole contributions.

### 7.1.2 Spin and Quadrupole Contributions to $\Sigma_z^n$

Fig. 14 exhibits that there are sizeable spin contributions to the asymmetry  $\Sigma_z^n$  for each angle, but for  $\theta = 110^\circ$  they nearly completely vanish below the pion production threshold. The reason is cancellation in the division of the difference (Fig. 15) by the sum (Fig. 6). This cancellation arises as the shape of the three curves in Fig. 15 for  $\theta = 110^\circ$  is nearly exactly symmetric to the three spin-averaged cross section curves at the same angle with respect to the  $\omega$ -axis. Therefore, dividing both results by each other hides the spin contribution. In the difference, one recognizes a decreasing spin dependence with increasing angle, which can again be explained by  $A_1$  and  $A_3$ . In forward direction,  $A_3^{\text{pole}}$  starts with a falling slope and stays negative for the energy range we are considering. Adding the structure part of  $A_3$ , i.e. including the spin polarizabilities, the amplitude changes sign roughly at the pion mass. Therefore we see a completely different behavior of  $A_1 \cdot A_3^{\text{pole}}$  and  $A_1 \cdot A_3$  in forward direction. In backward direction  $A_1$ ,  $A_3$  and  $A_3^{\text{pole}}$  are all positive below  $\omega_\pi$ , resulting in very similar curves.

As in the proton case we find the quadrupole part to be negligibly small within the accuracy of this analysis (Fig. 14).

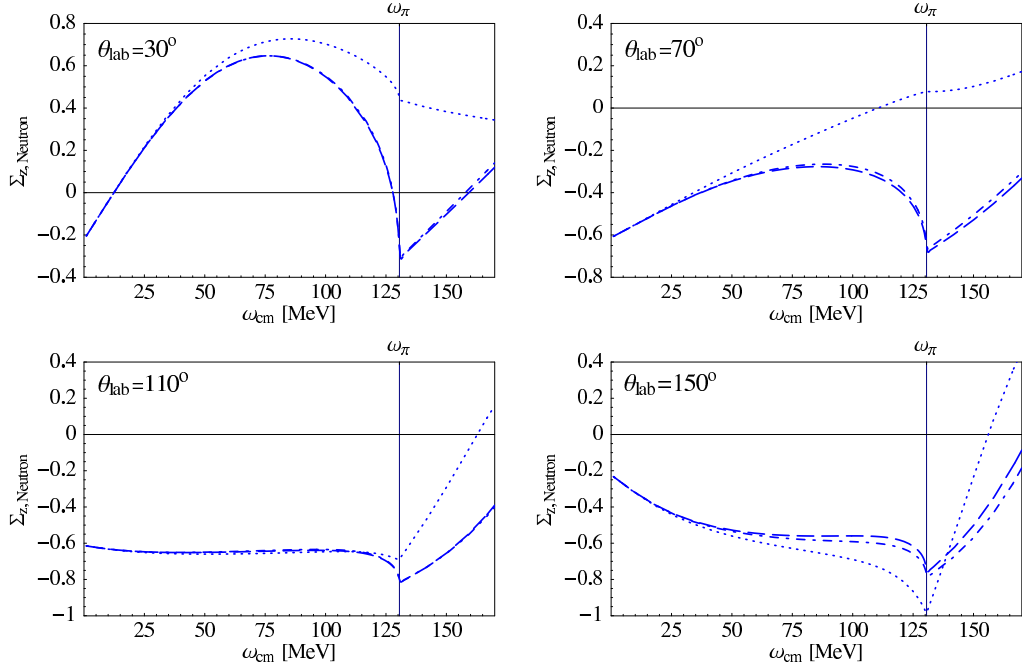


Figure 14: Complete  $\mathcal{O}(\epsilon^3)$ -SSE-predictions (dashed) for the neutron asymmetry  $\Sigma_z^n$ ; dotted: spin polarizabilities not included, dotdashed: quadrupole polarizabilities not included.

## 7.2 Nucleon Spin Perpendicular to Photon Momentum

### 7.2.1 Comparison: Pole-, HB $\chi$ PT- and SSE-calculation of $\Sigma_x^n$

The shape of the asymmetry  $\Sigma_x^n$  in Fig. 16 with the minimum at  $\omega_\pi$  is similar to  $\Sigma_z^n$  (Fig. 13), at least in forward direction. The curve is shifted downward with increasing angle  $\theta$ . An explanation for this behaviour can be given, though it is not obvious, as for  $\theta \approx 0^\circ$ ,  $\theta \approx 180^\circ$  there remain five terms in Eq. (3.3):  $[A_3(A_3 - A_1) \cos \theta + A_3 A_4 (1 + \cos^2 \theta) + A_3 A_5 (3 \cos^2 \theta - 1) + 2 A_3 A_6 \cos \theta] \sin \theta \approx [A_3(A_3 - A_1) \cos \theta + 2 A_3(A_4 + A_5 + A_6 \cos \theta)] \sin \theta$ . As can be read off Eq. (2.4), the leading pole terms – which are linear in  $\omega$  – vanish in the sum  $A_4 + A_5 + A_6 \cos \theta$ . Therefore the lowest order in  $\omega$  of  $A_3(A_4 + A_5 + A_6 \cos \theta)$  is  $\omega^4$ , since the spin-dependent structure amplitudes start with  $\omega^3$ . This is two orders in  $\omega$  above the leading order of  $A_3(A_3 - A_1) \cos \theta$ , which therefore is the leading term for small energies – at least for  $|\cos \theta| \gg 0$ . As discussed before, the product  $A_1 A_3$  is negative for low energies in forward direction, leading to a positive slope of the difference and therefore to positive values for the asymmetry. In backward direction,  $(A_3 - A_1)$ , as well as  $A_3$ , is positive, which gives a negative asymmetry as  $\cos \theta < 0$ . The angular dependence of the static value is determined by the pole contributions. It is

$$\Sigma_x^n(\omega = 0, \theta) = \frac{4 \sin \theta \cos \theta}{5 - \cos(2\theta)} , \quad (7.2)$$

but as for  $\Sigma_z^n$ , the dynamics of  $\Sigma_x^n$  is completely dominated by the neutron polarizabilities.

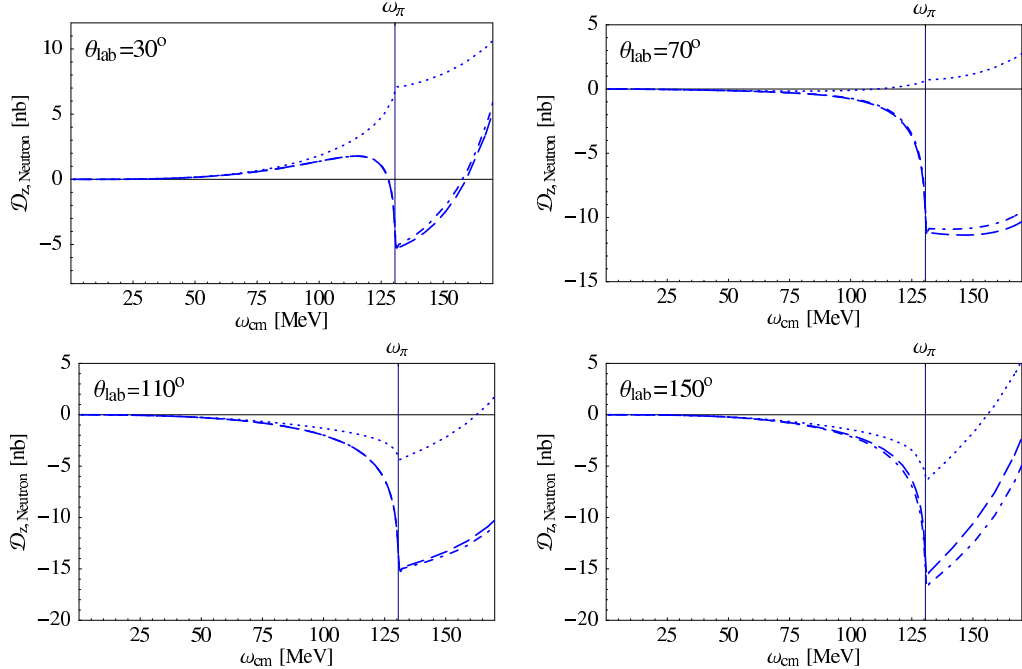


Figure 15: Complete  $\mathcal{O}(\epsilon^3)$ -SSE-predictions (dashed) for the neutron difference  $\mathcal{D}_z^n$ ; dotted: spin polarizabilities not included, dotdashed: quadrupole polarizabilities not included.

Another interesting feature in Fig. 16 is the fact, that the explicit  $\Delta$  degrees of freedom only play a minor role in forward direction but dominate for large angles.

### 7.2.2 Spin and Quadrupole Contributions to $\Sigma_x^n$

Turning to Figs. 17 and 18,  $\Sigma_x^n$  exhibits of all asymmetries by far the largest sensitivity on the spin polarizabilities. Therefore, an experiment with the nucleon spin aligned perpendicular to the photon momentum seems from the theorist's point of view to be the most promising of the considered configurations to extract the spin polarizabilities. The weakest dependence on the  $\gamma_i$ 's at low energies of  $\Sigma_x^n$  occurs in extreme forward direction. This again can be explained looking at  $A_1$  and  $A_3$  (Fig. 19): In the backward direction,  $A_3^{\text{pole}} < A_3$  and therefore also  $(A_3^{\text{pole}} - A_1) < (A_3 - A_1)$ , giving a much larger absolute value when spins are included. In the forward direction,  $A_3$  differs weakly from  $A_3^{\text{pole}}$  for  $\omega \leq 110$  MeV, so that spin polarizability effects appear only for higher energies.

As in  $\Sigma_z^n$ , the quadrupole polarizabilities in  $\Sigma_x^n$  are negligibly small (Fig. 17). One observes the strongest contributions around  $\theta = 90^\circ$ ; a simple answer to this phenomenon cannot be given, albeit it is clear that  $\Sigma_x^n$  should be most sensitive at a scattering angle around  $90^\circ$ , as the overall factor  $\sin \theta$  reaches its maximum (Eq. (3.3)), but this is a general feature and not only concerning the quadrupole polarizabilities.

So as a short conclusion of Sects. 6 and 7 we find a much stronger sensitivity of the neutron

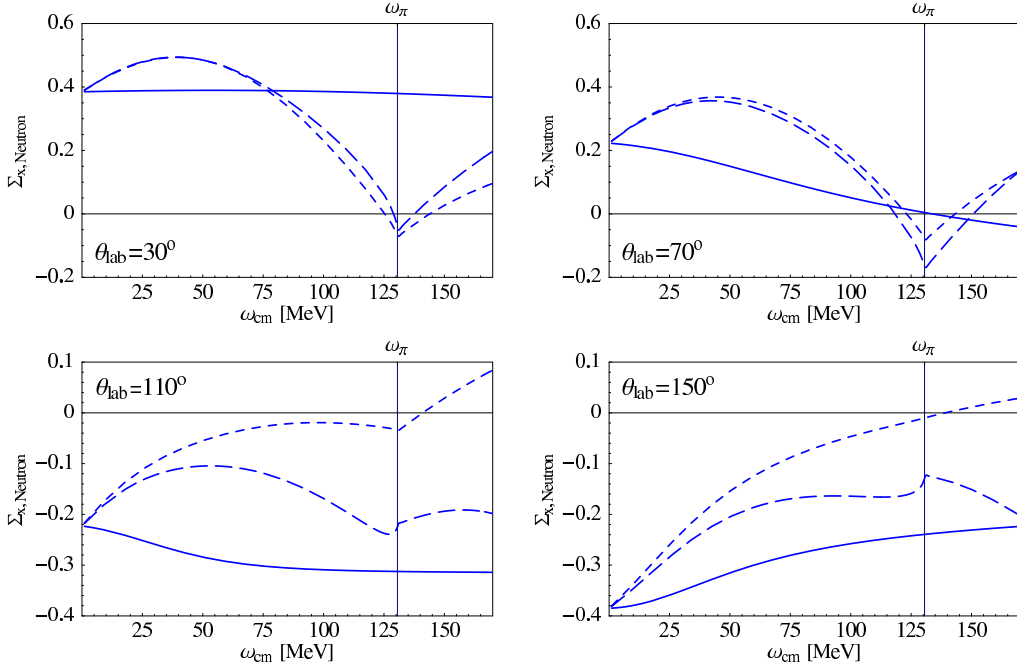


Figure 16:  $\mathcal{O}(p^3)$ -HB $\chi$ PT- (shortdashed) and  $\mathcal{O}(\epsilon^3)$ -SSE-predictions (longdashed) for the neutron asymmetry  $\Sigma_x^n$ ; the solid line describes the third order pole contributions.

asymmetries on the nucleon structure, while the proton asymmetries are dominated by pole terms up to at least 50 MeV. Contributions of the  $\Delta(1232)$  resonance are crucial only for certain asymmetries and angles. For both nucleons, the spin configuration  $\Sigma_x$  turned out to be more sensitive on the nucleon spin structure than  $\Sigma_z$ . Dynamical quadrupole contributions are negligible in each of the considered cases.

## 8 Conclusion

In this work, we examined spin-averaged and double polarized nucleon Compton cross sections in the framework of Chiral Effective Field Theory as a guideline for future experiments. Our goal was to identify those experimental settings which are most likely to be sensitive to the four leading spin polarizabilities of the proton and neutron. These quantities parameterize the stiffness of the nucleon spin against electro-magnetically induced deformations of definite multipolarity and non-zero frequency. Their energy dependence gives profound insight into the dispersive behavior of the internal degrees of freedom of the nucleon, caused by internal relaxation effects, baryonic resonances and mesonic production thresholds, see also [13, 12] for details.

In the spin-averaged cross sections, Sect. 5, we found significant deviations between predictions with and without spin polarizabilities. Therefore, spin-averaged experiments can contribute to a direct determination of *dynamical spin* polarizabilities from data, too.

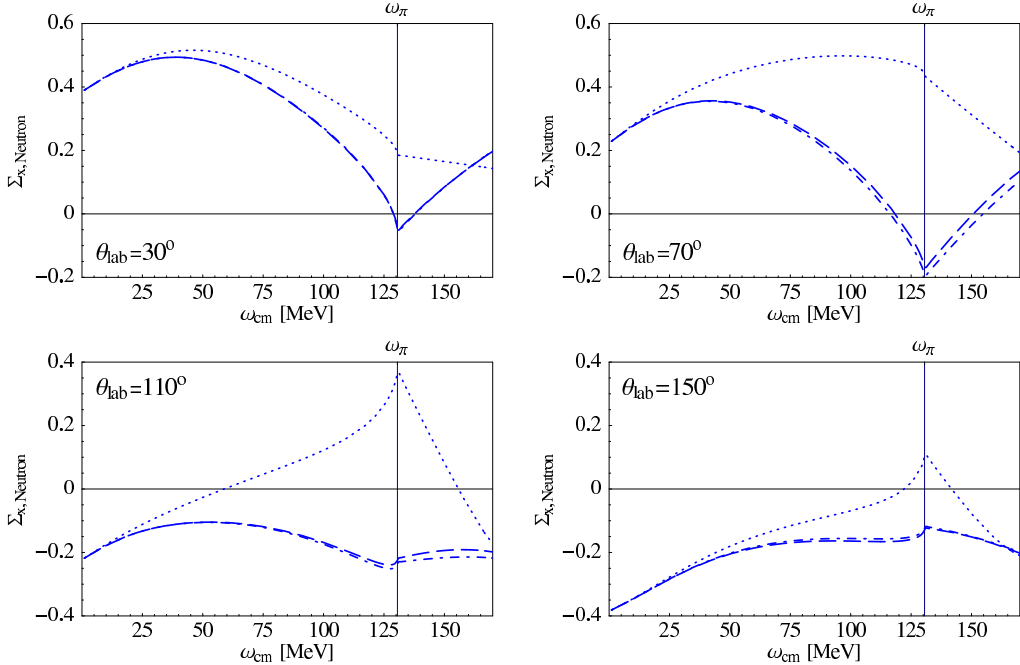


Figure 17: Complete  $\mathcal{O}(\epsilon^3)$ -SSE-predictions (dashed) for the neutron asymmetry  $\Sigma_x^n$ ; dotted: spin polarizabilities not included, dotdashed: quadrupole polarizabilities not included.

In the polarized case, Sects. 6 and 7, we considered configurations with a right-circularly polarized incident photon and a polarized target nucleon, leaving the spins of the particles in the final state undetected. We investigated the dependence of the cross sections and asymmetries on the spin polarizabilities in two different spin configurations: (i) nucleon spin parallel minus antiparallel to the photon momentum, and (ii) perpendicular to it but still inside the reaction plane. We noted a stronger sensitivity in the asymmetry  $\Sigma_x$  of configuration (ii) for both proton and neutron targets, than in case (i). We found furthermore that only two of the structure amplitudes, namely  $A_1$  and  $A_3$ , dominate all cross sections and asymmetries.

The spin polarizabilities give usually the clearest signal for photon energies above 100 MeV, say around the pion production threshold ( $\sim 130$  MeV), where most of the asymmetries also reach  $\mathcal{O}(1)$ . In backward direction, the neutron asymmetries also show a strong sensitivity on the physics of the  $\Delta(1232)$  resonance, in addition to contributions from the chiral pion cloud around the nucleon.

In general, the neutron asymmetries were found to be more sensitive to the spin polarizabilities than the proton analogs. This is no surprise, since Compton scattering on the charged proton is dominated by the pole amplitudes. Besides the resulting minor sensitivity on the nucleon structure, another disadvantage of the proton asymmetries is the small spin-averaged cross section around the pion production threshold for small angles, which enhances theoretical uncertainties. Again, we emphasize that up to leading-one-loop

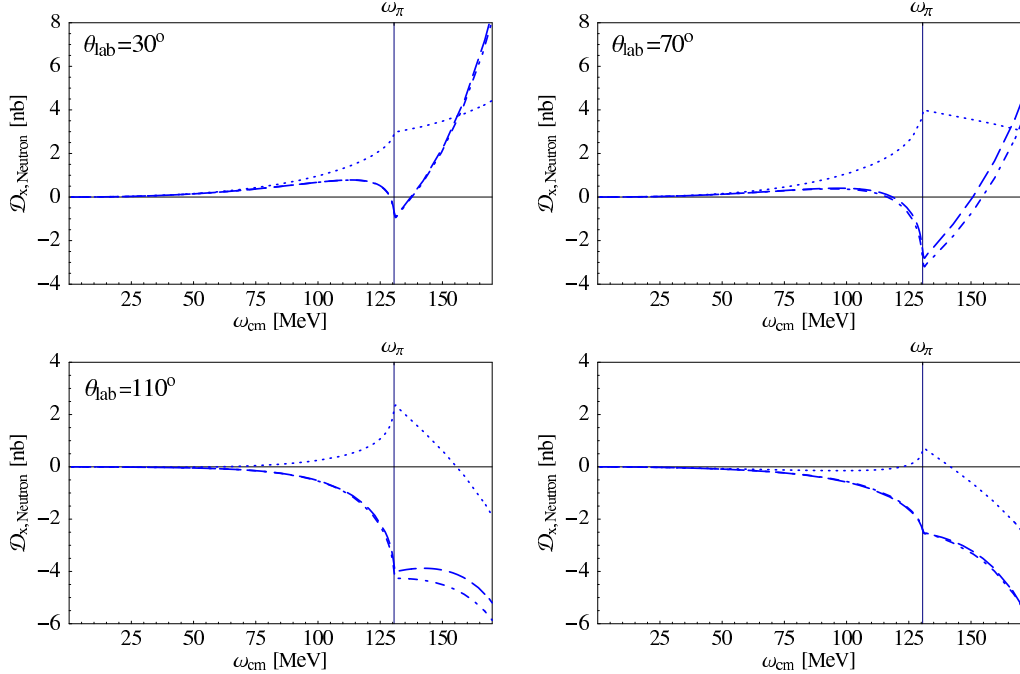


Figure 18: Complete  $\mathcal{O}(\epsilon^3)$ -SSE-predictions (dashed) for the neutron difference  $\mathcal{D}_x^n$ ; dotted: spin polarizabilities not included, dotdashed: quadrupole polarizabilities not included.

order the only difference between proton and neutron is given by the pole contributions, i.e. the structure part of our amplitudes is the one of an isoscalar nucleon. Polarized cross sections, which are calculated in this approximation, might therefore deviate from experimental results, especially for the neutron, where the pole contributions are weak. Hints on important isovector contributions are given in [22], where the non-pion-pole contribution to the backward spin polarizability  $\gamma_\pi$  of the neutron was found about twice as large as the corresponding proton value.

Contributions of the quadrupole polarizabilities turned out to be negligibly small, as in the spin-averaged case [13]. Therefore, like spin-averaged observables, spin-polarized cross sections are well described by only six energy-dependent functions: the two spin-independent and four spin dipole polarizabilities. This lead us in Sect. 4 to propose to extract the energy dependence of the four spin polarizabilities of the individual nucleons by a model-independent multipole expansion of the structure amplitudes from a combination of polarized and unpolarized precision experiments. Chiral Effective Field Theory with explicit  $\Delta(1232)$  degrees of freedom represents correctly the symmetries and low energy degrees of freedom inside the nucleon in a model-independent way. One can therefore in a first step accept our predictions of the energy dependence of the polarizabilities as induced by dispersive effects and only fit their overall normalization to experiment, thus obtaining their static values. At present, only two linear combinations,  $\gamma_0$  and  $\gamma_\pi$ , were measured experimentally on the proton at LEGS [6] and MAMI [7, 8], with partially conflicting values.

Clearly, the lack of free neutron targets makes an extension of the work presented here to light nuclei mandatory if experiments are to be interpreted, especially in the light of feasibility studies on Compton scattering on the deuteron and  $^3\text{He}$  at  $\text{HI}\gamma\text{S}/\text{TUNL}$  [15]. Work is therefore under way to consider spin polarized observables on these configurations, systematically including all binding and pion exchange current effects in an extension of Chiral Effective Field Theory to light nuclei [16]. Further investigations involving linearly polarized photon beams are also in preparation [16]. We are therefore confident that such future experiments will further our understanding of a fundamental property of the nucleon: the response of its effective low energy degrees of freedom, and in particular of its spin, in strong electric and magnetic fields, as parameterized in the dipole polarizabilities.

## Acknowledgments

The authors acknowledge helpful discussions with H. Gao and W. Weise. We are grateful to the ECT\* in Trento for its hospitality. This work was supported in part by the Bundesministerium für Forschung und Technologie, and by Deutsche Forschungsgemeinschaft under contract GR1887/2-1 (HWG and RPH).

## A Dominant Amplitudes at Low Energies

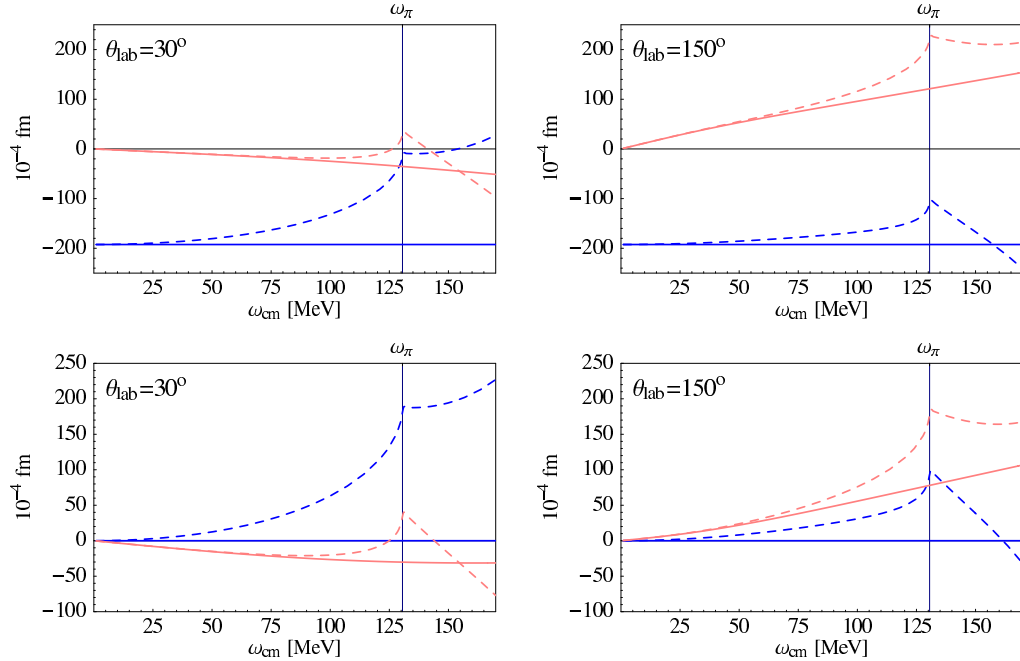


Figure 19:  $\mathcal{O}(\epsilon^3)$ -SSE-results for the real parts of the amplitudes  $A_1$  (blue/dark) and  $A_3$  (red/light); the dashed line is the full  $\mathcal{O}(\epsilon^3)$ -SSE-result, the solid line the third order pole contribution, given in Eqs. (2.3, 2.4); the upper (lower) panels show the proton (neutron) results. Recall that for the neutron,  $A_1^{\text{pole}} = 0$ .

In Fig. 19, we plot  $A_1$  and  $A_3$  at forward and backward angles, as we found in Sects. 5, 6 and 7 many low energy features in our results for polarized and unpolarized cross sections that can be explained by considering only those two amplitudes. The upper two panels in Fig. 19 show the plots for the proton in extreme forward and backward direction, the lower two the ones for the neutron.  $A_1$  is sketched dark/blue,  $A_3$  light/red. The solid lines are the pole contributions from Eq. (2.3) and Eq. (2.4), the dashed lines are the full (i.e. up to  $l = 2$ )  $\mathcal{O}(\epsilon^3)$ -results. The amplitudes of the uncharged neutron vanish for  $\omega = 0$  while the static value of  $A_1^p$  is given by the Thomson limit.

The clear cusp structure arises from  $\alpha_{E1}(\omega)$  in  $A_1$  and from  $\gamma_{E1E1}(\omega)$  in  $A_3$ , cf. Eq. (2.2) and [13].

## References

- [1] D. Drechsel, B. Pasquini and M. Vanderhaeghen, Physics Reports 378, 100 (2003).
- [2] B.R. Holstein “Chiral Perturbation Theory and Nucleon Polarizabilities”, in Chiral Dynamics 1997: Theory and Experiment, Editors: A.M Bernstein, D. Drechsel and T. Walcher, Springer-Verlag, Berlin (1998). [[hep-ph/9710548](#)].
- [3] T.R. Hemmert, “Nucleon Compton Scattering in Chiral Effective Field Theories”, in Chiral Dynamics 2000: Theory and Experiment. Eds.: A.M. Bernstein, J. Goity and U.-G. Meißner, World Scientific, Singapore (2001). [[nucl-th/0101054](#)].
- [4] S. Ragusa, Phys. Rev. D 47, 3757 (1993).
- [5] J. Ahrens et al. [GDH Collaboration], Phys. Rev. Lett. 87, 022003 (2001).
- [6] J. Tonnison, A.M. Sandorfi, S. Hoblit and A.M. Nathan, Phys. Rev. Lett. 80, 4382 (1998).
- [7] V. Olmos de Leon et al., Eur. Phys. J. A 10, 207 (2001).
- [8] G. Galler et al., Phys. Lett. B 503, 245 (2001).
- [9] S. Wolf et al., Eur. Phys. J. A 12, 231 (2001).
- [10] M. Camen et al., Phys. Rev. C 65, 032202(R) (2002).
- [11] T.R. Hemmert, B.R. Holstein, J. Kambor and G. Knöchlein: Phys. Rev. D 57, 5746 (1998).
- [12] H.W. Grießhammer and T.R. Hemmert, Phys. Rev. C 65, 045207 (2002).
- [13] R.P. Hildebrandt, H.W. Grießhammer, T.R. Hemmert and B. Pasquini, [nucl-th/0307070](#).
- [14] D. Babusci, G. Giordano, A.I. L’vov, G. Matone and A.M. Nathan, Phys. Rev. C 58, 1013 (1998).
- [15] H. Gao, private communication (2002, 2003).
- [16] R.P. Hildebrandt et al., in preparation.
- [17] V. Bernard, N. Kaiser and U.-G. Meißner, Int. J. Mod. Phys. E 4, 193 (1995).
- [18] T.R. Hemmert, B.R. Holstein and J. Kambor, J. Phys. G 24, 1831 (1998).
- [19] Particle Data Group, Review of Particle Physics, Phys. Rev. D 66, 010001 (2002).
- [20] V. Bernard, N. Kaiser, J. Kambor and U.-G. Meißner, Nucl. Phys. B 388, 315 (1992).

- [21] T.R. Hemmert, B.R. Holstein and J. Kambor, Phys. Rev. D 55, 5598 (1997).
- [22] K. Kossert et al., Eur. Phys. J. A 16, 259 (2003).